Progress In Electromagnetics Research B, Vol. 88, 197–215, 2020

Optimum Design Methodology for Axially Polarized Multi-Ring Radial and Thrust Permanent Magnet Bearings

Siddappa I. Bekinal[1, *] and Mrityunjay Doddamani[2]

Abstract—This article deals with the generalized procedure of designing and optimizing multi-ring radial and thrust permanent magnet bearings (PMBs) with an axial air gap for maximum force and stiffness per volume of the magnet. Initially, the procedure of determining optimized design variables in both the configurations is presented using the MATLAB codes written for solving the three dimensional (3D) equations of force and stiffness in PMB having 'n' number of rings on the stator and rotor. The maximized results of the forces in both radial and thrust multi-ring PMBs are validated with the values obtained using finite element analysis (FEA). Then, the correlation between the optimized parameters and the air gap is obtained, and curve fit equations for the same are proposed in terms of stator outer diameter. Further, curve fit equations establishing the relationship between the maximized bearing features, and the aspect ratio (L/D4) of the bearing are expressed for different values of air gap in both the radial and thrust bearings. Finally, the generalized method of designing and optimizing the multi-ring PMB is demonstrated with a specific application. A designer can use the presented curve fit equations for optimizing design variables and calculating maximized bearing features in multi-ring radial and thrust PMBs easily just by knowing the bearing features for a single ring pair.

1. INTRODUCTION

Permanent magnet bearings (PMBs) [1–4] are friction, lubrication, and maintenance-free bearings wherein the levitation of the moving device is due to the attractive or repulsive forces of the magnets fitted on stationary and moving components. PMBs do not require any input energy, sensors, electrical and electronics components to perform their function as compared to active magnetic bearings. Due to these attractive features, PMBs have been utilized to support both low [5, 6] and high-speed [7–11] rotors in different applications. The mathematical equations addressing force and stiffness characteristics in single as well as multi-ring radial [12–15] and thrust [16–19] PMBs have been presented in the literature. To obtain characteristics of PMBs as comparable with conventional bearing characteristics, the optimization of their geometrical dimensions for maximum features is necessary. Moser et al. [20] demonstrated the optimization of bearing dimensions in a multi-ring radial PMB using finite element analysis (FEA). In [21], a pragmatic optimization of axially magnetized and rotational magnetized direction (RMD) configurations was performed for maximum bearing capacity. Equations for mean radius and clearance were given to help the designers in the industry in terms of length and outer diameter of the bearing for the maximum radial load. Multi-objective optimization of radial PMB for maximum features was reported by Lijesh et al. [22], and the equations were presented for optimized variables for multi-ring structure in terms of a single ring in a given volume. In [23], the authors used 2D analytical equations for optimizing different multi-layer thrust PMB structures for maximum characteristics. Bekinal et al. [24, 25] presented the optimization of conventional and RMD structures

Received 5 September 2020, Accepted 14 October 2020, Scheduled 23 October 2020
* Corresponding author: Siddappa Iranna Bekinal (siddappabekinal@gmail.com).
[1] Department of Mechanical and Manufacturing Engineering, Manipal Institute of Technology, Manipal Academy of Higher Education, Manipal-576104, Udupi, Karnataka, India. [2] Department of Mechanical Engineering, National Institute of Technology Karnataka, Surathkal-575025, Mangalore, Karnataka, India.

of multi-ring thrust PMBs using 3D equations and presented the generalized curves for the design variables in terms of the air gap. Despite the attractive features, the major issue associated with PMB is low damping. Active [26], as well as passive dampers [27, 28], could be used to increase damping in PMB. The use of active dampers makes the bearing system bulky due to the presence of electronic components. Viscoelastic or eddy current type can be used as passive dampers in PMB. Eddy current dampers (ECDs) are formed by inserting conductive material in the radial air gap of PMB. An increase in the air gap due to conductive materials in passive dampers decreases the characteristics of PMB. The authors in [29, 30] pointed out that an optimal axial air gap exists for maximum characteristics in axially magnetized multi-ring thrust PMB, and the same could be utilized to include conductive material to form ECD. Three-dimensional equations for an axial force and stiffness in multi-ring thrust PMB with an axial air gap between successive rings and optimization of design parameters were presented in our earlier efforts [31]. Based on the review of recent research contributions on the optimization of radial and thrust multi-ring PMBs, the following observations are made:

- The development of 3D equations for calculating characteristics in multi-ring radial PMB with an axial air gap between successive rings has not been reported in the literature.
- The optimization of multi-ring radial PMB has not been addressed so far by providing an axial air gap between the adjacent ring magnets.
- The generalization of an optimum design methodology in both multi-ring PMBs with an axial air gap in a given volume of the magnet is not presented.
- The general design procedure for the selection of optimized radial and thrust multi-ring PMBs in the industry for different applications is not addressed in the literature.

This article presents (i) the general 3D equations for force and stiffness in both radial and thrust multi-ring PMBs with an axial air gap, (ii) optimization of the bearing configuration as both radial and thrust PMBs for maximum force and stiffness, and validation of maximum axial and radial forces generated with FEA results, (iii) generalization of optimization procedure and presenting curve fit equations for the design variables, forces, and stiffness's in both the configurations, (iv) demonstration of the general optimum design methodology with application examples.

2. MULTI-RING PERMANENT MAGNET BEARING CONFIGURATIONS

Single ring pair radial and thrust bearing configurations are presented in Figs. 1(a) and 1(b). In a single ring pair PMB, the inner ring is fitted to the rotor and the outer one to the stator. The magnetic polarization of both the rings of radial bearing is in the same direction, whereas in a thrust bearing the polarization direction of the rotor ring is opposite to that of the stator. The rotor ring is levitated due to the repulsive and attractive forces between the faces of the magnet. The dimensions of the rotor and stator rings of the aforementioned configurations selected for the analysis are listed in Table 1. The single ring pair of the bearing can be replaced with several ring pairs to form a multi-ring structure to enhance the bearing characteristics. In multi-ring PMB, magnet rings are stacked one adjacent to other on both rotor and stator in the axial direction. The rings of the stator and rotor are polarized in alternate opposite axial directions to form radial and thrust bearings as shown in Figs. 1(c) and 1(d). The magnitude of the forces exerted on the rotor increases due to the number of rings on both stator and rotor of multi-ring structures.

3. MATHEMATICAL MODELING

The general mathematical equation for the radial force generated on the inner rings by the outer ones in multi-ring PMB structures is given by Equation (1). In the selected bearing configuration, an air gap is provided between the successive stacks of permanent magnet rings in the axial direction. The total radial force generated is the algebraic summation of the interaction forces among all the magnetized surfaces of rings fitted on both stator and rotor. The forces of interactions between the faces u^{th} ring fitted to a rotor and v^{th} ring to a stator in multi-ring radial PMB are shown in Fig. 2.

$$\mathrm{F_r} = \frac{B_r^2}{4\pi\mu_0} \sum_{\mathrm{u=1}}^{\mathrm{n}} \sum_{\mathrm{v=1}}^{\mathrm{n}} \sum_{\mathrm{k=1}}^{2} \sum_{\mathrm{l=3}}^{4} \sum_{\mathrm{p=1}}^{\mathrm{m}} \sum_{\mathrm{q=1}}^{\mathrm{m}} \frac{\mathrm{S_{pku} S_{qlv}}}{\mathrm{R^3}} \mathbf{R_{(pku)(qlv)}} \, (-1)^{(\mathrm{k+l})} \, (-1)^{(\mathrm{u+v})} \qquad (1)$$

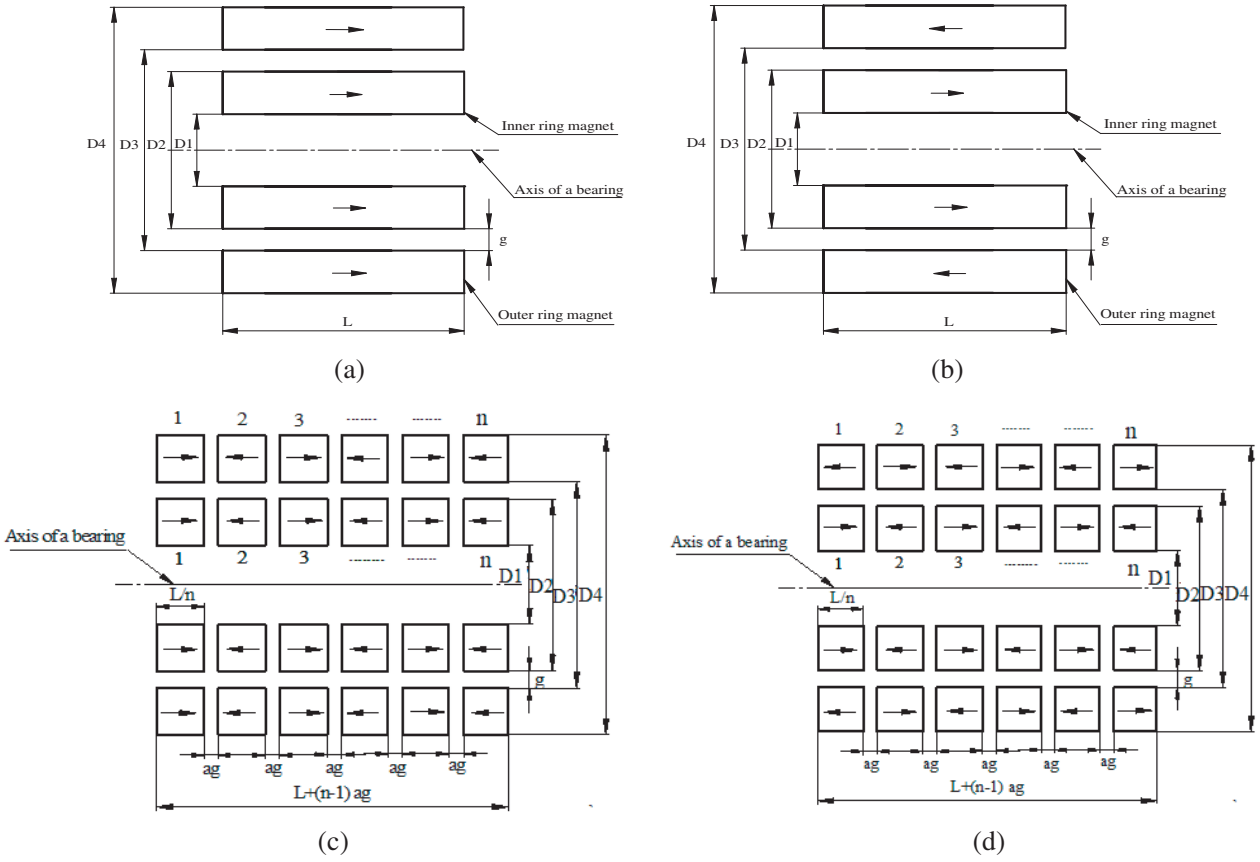

Figure 1. PMB configurations, (a) monolithic radial bearing, (b) monolithic thrust bearing, (c) multi-ring radial bearing, (d) multi-ring thrust bearing.

Table 1. Selected dimensions of PMB with one ring pair.

Parameter	Value
Inside diameter of rotor ring magnet, D1 (mm)	24
Outside diameter of rotor ring magnet, D2 (mm)	54
Inside diameter of stator ring magnet, D3 (mm)	58
Outside diameter of stator ring magnet, D4 (mm)	90
Air gap thickness, g (mm)	2
Length of magnet, L (mm)	45
Magnetic polarization, B_r (T)	1.2

where $\mathrm{R} = \sqrt{(\mathrm{X_{qlv}} - \mathrm{X_{pku}})^2 + (\mathrm{Y_{qlv}} - \mathrm{Y_{pku}})^2 + (\mathrm{Z_{qlv}} - \mathrm{Z_{pku}})^2}$ and $\mathbf{R_{(pku)(qlv)}} = (\mathrm{X_{qlv}} - \mathrm{X_{pku}})\mathbf{i} + (\mathrm{Y_{qlv}} - \mathrm{Y_{pku}})\mathbf{j} + (\mathrm{Z_{qlv}} - \mathrm{Z_{pku}})\mathbf{k}$ is the position vector. The coordinates of elements on the faces of magnets are,

$$
\begin{aligned}
(\mathrm{X_{pku}})_{1,2} &= (\mathrm{x} + \mathrm{r_{mr}} \cos\beta)\mathbf{i} & (\mathrm{X_{qlv}})_{3,4} &= (\mathrm{r_{ms}} \cos\alpha)\mathbf{i} \\
(\mathrm{Y_{pku}})_{1,2} &= (\mathrm{y} + \mathrm{r_{mr}} \sin\beta)\mathbf{j} & (\mathrm{Y_{qlv}})_{3,4} &= (\mathrm{r_{ms}} \sin\alpha)\mathbf{j} \\
(\mathrm{Z_{pku}})_{1} &= ((\mathrm{u}-1)\,\mathrm{l} + (\mathrm{u}-1)\,\mathrm{ag})\mathbf{k} & (\mathrm{Z_{qlv}})_{\mathbf{3}} &= ((\mathrm{v}-1)\mathrm{l} + (\mathrm{v}-1)\,\mathrm{ag})\,\mathbf{k} \\
(\mathrm{Z_{pku}})_{2} &= ((\mathrm{u})\,\mathrm{l} + (\mathrm{u}-1)\,\mathrm{ag})\mathbf{k} & (\mathrm{Z_{qlv}})_{\mathbf{4}} &= (\mathrm{vl} + (\mathrm{v}-1)\,\mathrm{ag})\,\mathbf{k}
\end{aligned}
\tag{2}
$$

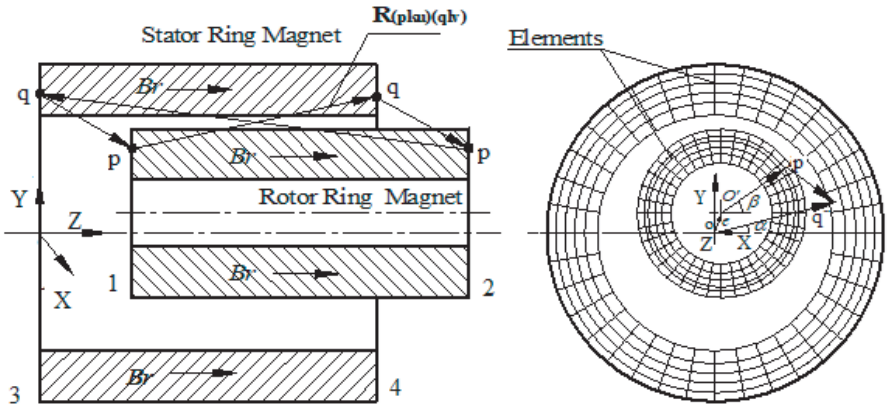

Figure 2. Magnetic interaction between two rings in multi-ring radial PMB.

Suffix 1, 3, and 2, 4 are the left and right surfaces of the rotor and stator, respectively. The thrust bearing is obtained by reversing the polarization direction of either the inner or outer ring of the configuration (Fig. 2). Equation (1) can be used to determine the axial force (F_z) generated in the multi-ring thrust PMB as shown in Fig. 1(d), and the corresponding coordinates of the elements are given in Equation (3).

$$
\begin{aligned}
(X_{pku})_{1,2} &= (r_{mr}\cos\beta)\mathbf{i} & (X_{qlv})_{3,4} &= (r_{ms}\cos\alpha)\mathbf{i} \\
(Y_{pku})_{1,2} &= (r_{mr}\sin\beta)\mathbf{j} & (Y_{qlv})_{3,4} &= (r_{ms}\sin\alpha)\mathbf{j} \\
(Z_{pku})_{1} &= (z+(u-1)\,l+(u-1)\,ag)\mathbf{k} & (Z_{qlv})_{\mathbf{3}} &= (\,(v-1)l+(v-1)\,ag)\,\mathbf{k} \\
(Z_{pku})_{2} &= (z+(u)\,l+(u-1)\,ag)\mathbf{k} & (Z_{qlv})_{\mathbf{4}} &= (vl+(v-1)\,ag)\,\mathbf{k}
\end{aligned}
\tag{3}
$$

The stiffnesses (K_r and K_z) in the radial and axial directions of the proposed multi-ring PMB structures are given by,

$$K_r = \frac{dF_r}{dr} \qquad K_z = \frac{dF_z}{dz} \tag{4}$$

4. OPTIMIZATION

In multi-ring PMB, bearing features can be maximized by optimizing the design variables. The bearing parameters considered for the process of optimization are air gap (g), number of axial stacks (n), axial offset (z), axial air gap (ag), inner diameters of rotor and stator rings (D1 and D3). Optimization could be performed in two ways: first, required bearing characteristics are achieved by minimizing magnet volume, and bearing features are maximized per given volume of the magnet in the second case. In this work, bearing features (force and stiffness) are maximized for the given volume of the magnet. The method of optimization in multi-ring PMB consists of the following steps:

1. In PM thrust bearings, the values of bearing characteristics vary with the axial offset of the rotor with reference to the stator. Initially, the range of axial offset values is fixed for calculating the characteristics. Similarly, in radial bearings, the characteristics increase with an increase in the radial displacement of the rotor magnets, and an eccentricity ratio of ε (e/g) = 0.5 is selected for the optimization.
2. The optimum number of rings for maximum bearing characteristics in the given volume of the magnet is determined by varying its value for the selected range of axial offset in thrust bearing and for the chosen eccentricity ratio in a radial bearing.
3. The optimum values of the axial air gap are calculated by fixing the optimized number of rings in the given volume of magnet obtained in the previous step, and this process is followed separately for force and stiffness in both radial and thrust PMBs.

4. As the bearing characteristics and optimized values of 'n' and 'ag' are predominantly dependent on the air gap, its value is increased from 0.2 to 3 mm with an increment of 0.2 mm in both radial and thrust bearings.
5. The optimization of the inside diameter of rotor magnet rings is carried out for the considered values of air gap by fixing the optimized values calculated in steps 2 to 4.
6. Finally, optimization of the inside diameter of stator rings is carried out at optimized values of 'n', 'ag', and 'D1' for the selected range of air gap values.

Optimization of radial and thrust bearing configurations selected in Section 2 and dimensions given in Table 1 are presented in the following section.

4.1. Multi-Ring Radial Bearing

The variation of radial force and stiffness values with the variables (number of axial stacks, axial air gap, and inside diameter of rotor and stator rings) selected for the optimization in the assumed volume of the magnet for different air gap values is shown in Figs. 3(a)–3(h). The optimized dimensions of the radial bearing are shown in Table 2. The change of maximized radial force and radial stiffness values with a radial displacement of the rotor in the optimized configuration along with the results of a selected radial bearing are shown in Fig. 4. It can be observed that the maximized value of radial force is 8.73 (458.72 N) times and stiffness is 9.8 (508450 N/m) times of the radial force and stiffness of the selected monolithic bearing at a radial offset of 1 mm.

Table 2. Optimized dimensions of multi-ring radial PMB.

Parameter	For Max. Fr	For Max. Kr
Inside diameter of rotor ring magnets, D1 (mm)	26	29
Outside diameter of rotor ring magnets, D2 (mm)	72	73
Inside diameter of stator ring magnets, D3 (mm)	76	77
Outside diameter of stator ring magnets, D4 (mm)	90	90
Air gap thickness, g (mm)	2	2
Axial air gap, ag, (mm)	1	0.8
Length of bearing, L (mm)	45	45
Number of axial stacks, n	7	8

4.2. Multi-Ring Thrust Bearing

The thrust bearing characteristics variations versus the variables (number of axial stacks, axial air gap, and inside diameter of rotor and stator magnet rings) selected for the optimization in the assumed volume of the magnet for different air gap values are shown in Figs. 5(a)–5(h). The optimized dimensions of thrust bearing for maximum force and stiffness are given in Table 3. Fig. 6 shows the variation of maximized features with an axial offset of the rotor in the optimized configuration along with results calculated for the selected thrust bearing. It can be seen that the maximized value of axial force is 4.1 (2343.16 N) times of the axial force, and stiffness is 7.95 (800557.3 N/m) times of the stiffness developed in the monolithic bearing.

5. VALIDATION OF MATHEMATICAL MODEL RESULTS

The permanent magnet rings with optimized dimensions (Table 2 & Table 3) are modelled in ANSYS by providing optimized values of an axial air gap between successive rings on both stator and rotor. N35 grade magnet rings with properties $B_r = 1.2$ T, coercive force $H_c = 868$ kA/m, and relative

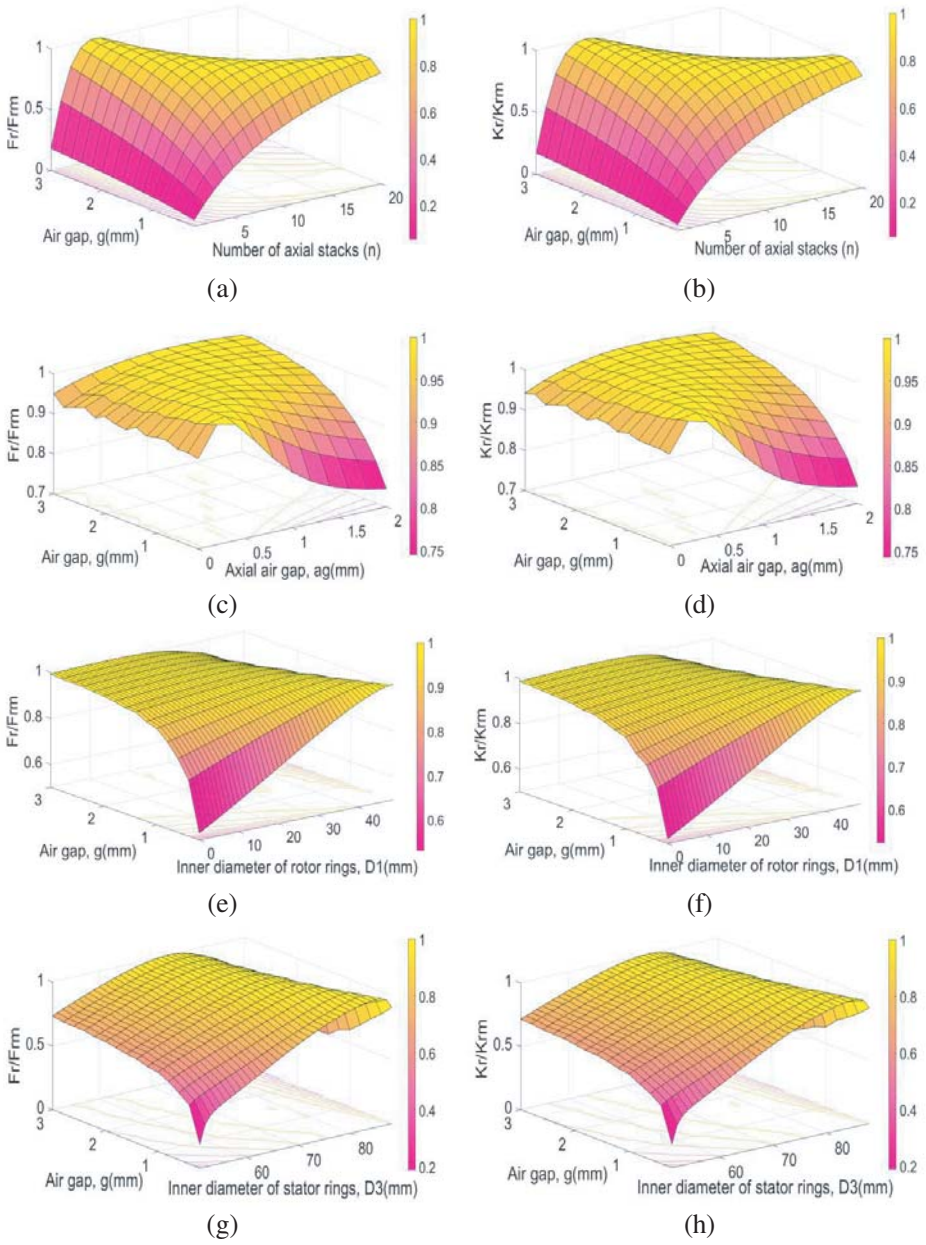

Figure 3. Variation of radial bearing characteristics, (a) Fr Vs n, (b) Kr Vs n, (c) Fr Vs ag, (d) Kr Vs ag, (e) Fr Vs D1, (f) Kr Vs D1, (g) Fr Vs D3, (h) Kr Vs D3.

permeability, $\mu_r(B_r/\mu_0 H_c) = 1.2\,\mathrm{T}$ are selected for the analysis of both radial and thrust bearings. Both configurations are created using solid97 elements, and rings of the bearing are magnetized in alternately opposite directions (Figs. 7(a) and 8(a)). The radially displaced rotor rings in radial bearing are shown in Fig. 7(b), and flux lines of the rings of thrust bearing are depicted in Fig. 8(b). The force generated in the bearings is determined using the magnetic virtual displacement method, and the maximum forces developed in radial and thrust bearings are shown in Figs. 7(c) and 8(c). The maximum value of radial force generated using FEA is 440.57 N, which is in close agreement with the force (458.7 N) calculated using a mathematical model at an eccentricity ratio of 0.5. Axial force values calculated using the mathematical model and FEA, in the optimized thrust bearing at different axial offset values, are plotted in Fig. 8(d). Deviation of 8.24% is observed between the maximum values of an axial force (2317 N & 2126.6 N) at $z = -10\,\mathrm{mm}$.

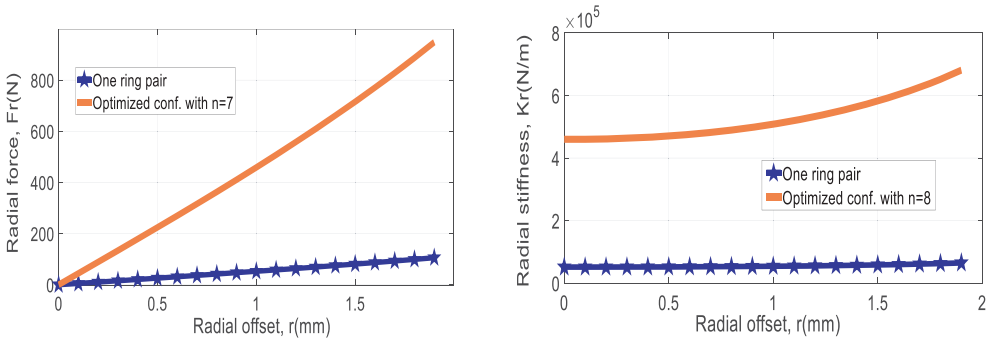

Figure 4. Comparison of maximized characteristics in radial bearing, (a) Fr Vs r, (b) Kr Vs r.

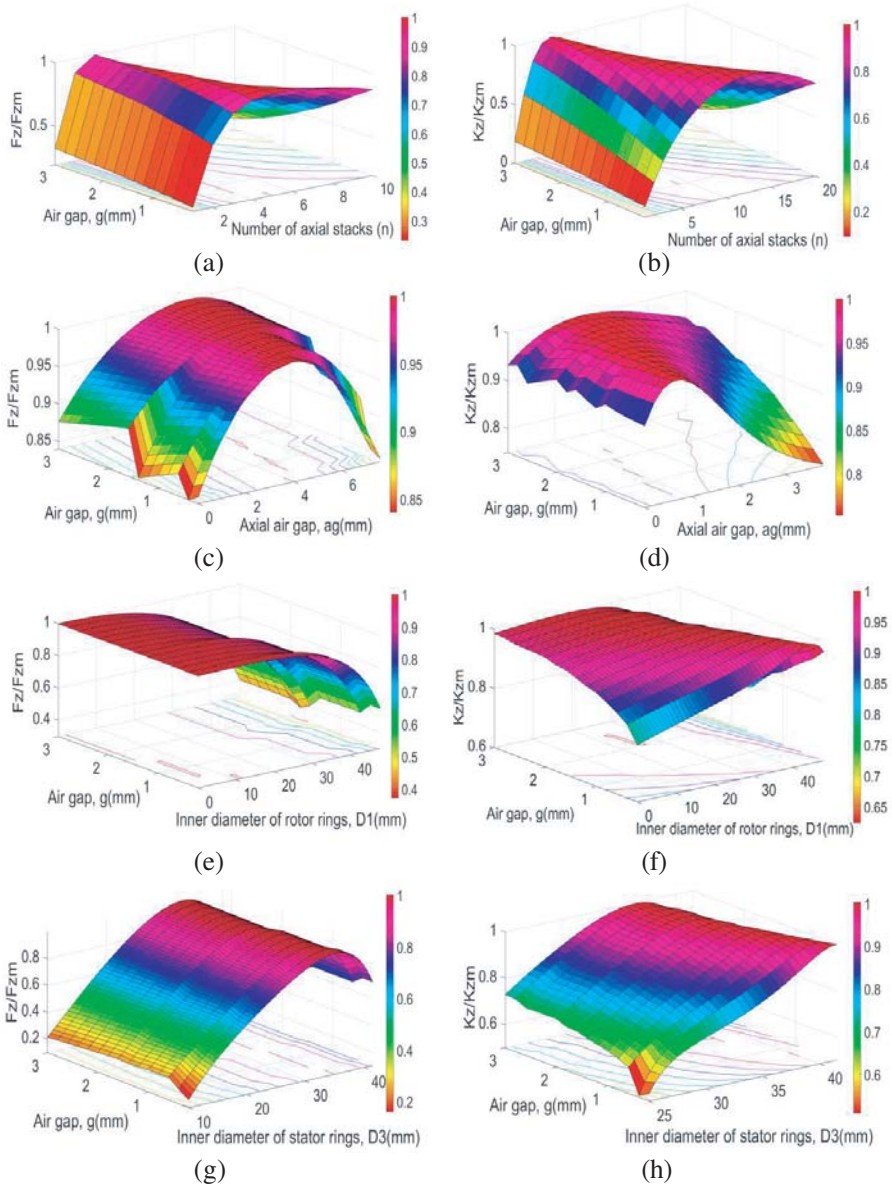

Figure 5. Variation of thrust bearing characteristics, (a) Fz Vs n, (b) Kz Vs n, (c) Fz Vs ag, (d) Kz Vs ag, (e) Fz Vs D1, (f) Kz Vs D1, (g) Fz Vs D3, (h) Kz Vs D3.

Table 3. Optimized dimensions of multi-ring thrust PMB.

Parameter	For Max. Fz	For Max. Kz
Inside diameter of rotor ring magnets, D1 (mm)	2	26
Outside diameter of rotor ring magnets, D2 (mm)	62	72
Inside diameter of stator ring magnets, D3 (mm)	66	76
Outside diameter of stator ring magnets, D4 (mm)	90	90
Air gap thickness, g (mm)	2	2
Axial air gap, ag, (mm)	5.2	1.2
Axial length, L (mm)	45	45
Number of axial stacks, n	3	6

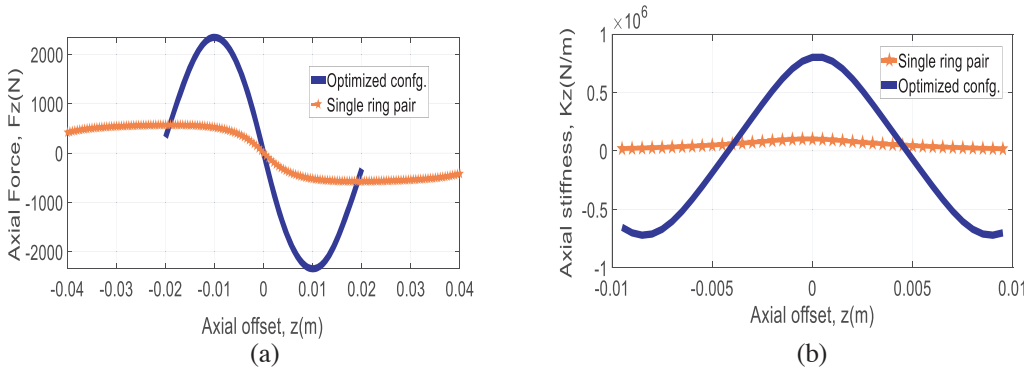

Figure 6. Comparison of maximized characteristics in thrust bearing, (a) Fz Vs z, (b) Kz Vs z.

6. GENERALIZATION OF OPTIMUM DESIGN METHODOLOGY

This section presents the generalization of an optimal design methodology for multi-ring radial and thrust PMBs. The generalization is carried out by establishing the relation between optimum design variables (Ho, ago, D1o and D3o) and an air gap (g) in terms of the outer diameter of a stator (D4) and providing curve fit equations for all optimum design variables in terms of an air gap. The plots showing the relationship and curve fit equations for optimized design variables in multi-ring radial PMB are shown in Figs. 9(a)–9(d) and 10(a)–10(d). The plots and curve fit equations in multi-ring thrust bearing are depicted in Figs. 11(a)–11(d) and 12(a)–12(d).

After presenting the generalized curve fit equations for the optimum design variables in radial and thrust PMBs, the relationship between maximum bearing characteristics and aspect ratio for different air gaps can be established. The same could be done by selecting new bearing configurations having different values of aspect ratio and air gap. The dimensions of new radial and thrust bearing selected for the analysis are given in Tables 4 and 5. The optimum design variables in the selected configurations are determined by using the presented corresponding curve fit equations, and maximum force and stiffness values are calculated using Equations (1) and (4) given in the mathematical model.

The relationships between the ratio of the maximized value of the radial force of the optimized configuration and maximized value of radial force in a single ring configuration (Frm/Frms) and L/D4 along with curve fit equations for different air gap values are shown in Figs. 13(a)–(e), and those between the ratio of the maximized value of radial stiffness of the optimized configuration and maximized value of radial stiffness in a single ring configuration (Krm/Krms) and L/D4 in radial bearing are depicted in Figs. 14(a)–14(e).

In thrust PMB, the relationships between the ratio of the maximized value of an axial force in the optimized bearing and maximized value of axial force in a single ring configuration (Fzm/Fzms) and

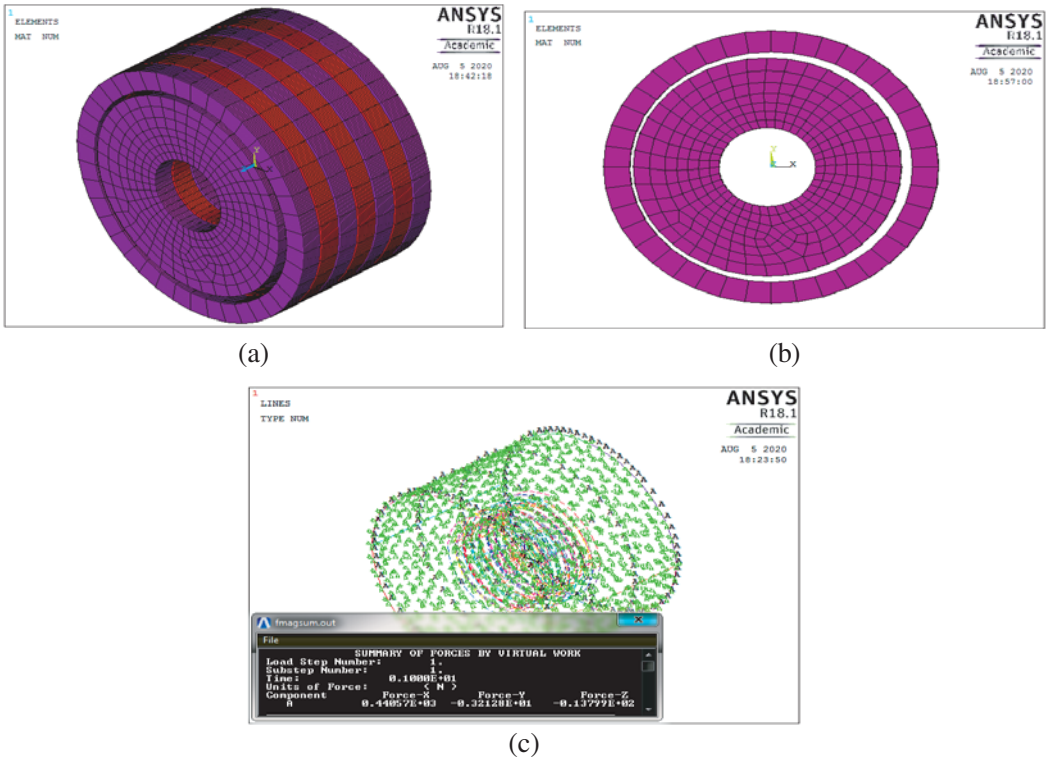

Figure 7. FEA results of an optimized multi-ring radial PMB, (a) modelling of rotor and stator rings, (b) radial displacement of rotor rings with respect to stator rings, (c) maximum radial force generated on inner rings.

Table 4. Dimensions of a radial PMB.

Air gap, g (mm)	Outer diameter of the stator, D4 (mm)
0.5	100
1.0	
1.5	
2.0	
2.5	
Values of an axial length (L) of bearing is taken as 25, 50, 75, 100, 125, and 150 mm for each air gap value to have an aspect ratio (L/D4) as 0.25, 0.5, 0.75, 1.0, 1.25, and 1.5.	

L/D4 along with curve fit equations for different air gap values are shown in Figs. 15(a)–15(e), and those between the ratio of the maximized value of axial stiffness of the optimized configuration and maximized value of axial stiffness in a single ring configuration (Kzm/Kzms) and L/D4 are shown in Figs. 16(a)–16(e).

7. APPLICATION EXAMPLES

In this section, the general optimum design methodology for radial and thrust PMBs for maximum bearing features is demonstrated with examples. Different steps involved in selecting and optimizing multi-ring radial and thrust PMBs for different applications in the industry are given below:

1. Choose the particular values for the ratios g/D4 and L/D4 among the values selected in the

Table 5. Dimensions of a thrust PMB.

Air gap, g (mm)	Outer diameter of the stator, D4 (mm)
0.5	80
1.0	
1.5	
2.0	
2.5	
Values of an axial length (L) of bearing is taken as 20, 40, 60, 80, 100 and 120 mm for each air gap value to have an aspect ratio (L/D4) as 0.25, 0.5, 0.75, 1.0, 1.25, and 1.5.	

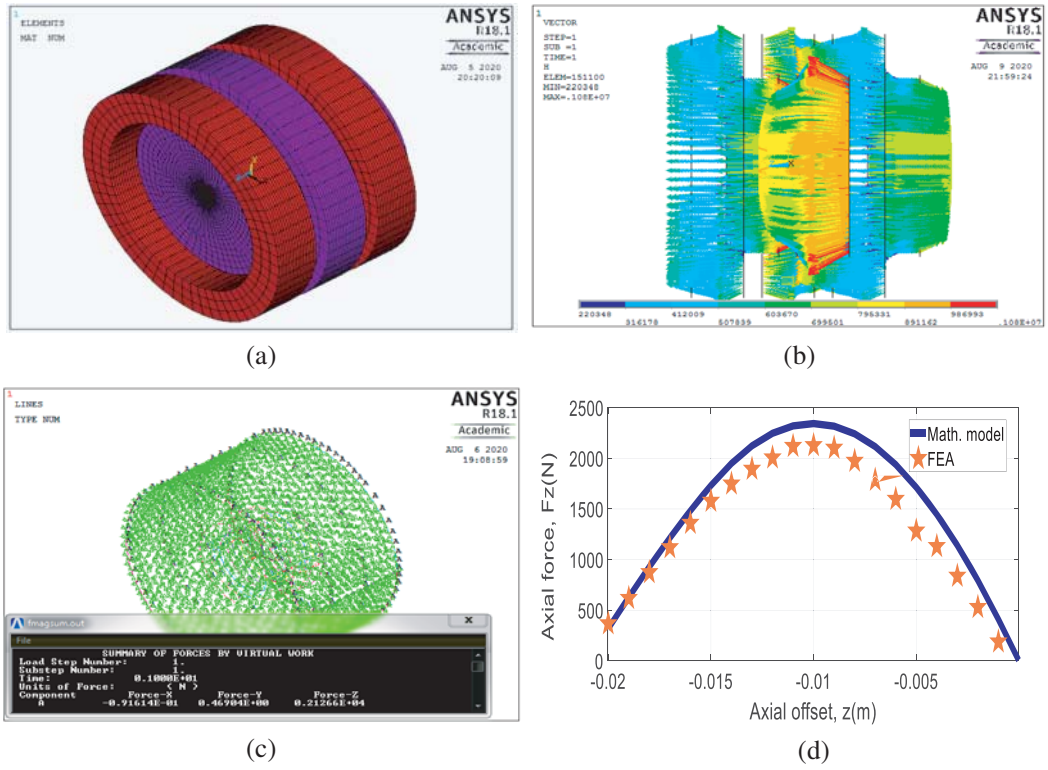

Figure 8. FEA results of an optimized multi-ring thrust PMB, (a) modelling of stator and rotor rings, (b) magnetic flux lines of rotor and stator magnets, (c) maximum axial force generated at z = −10 mm, (d) comparison of FEA and mathematical model results.

generalization of the optimization procedure.

2. Select the value of the air gap (g) according to the design requirements and calculate the outer diameter (D4) and length (L) of the bearing.
3. Then, the optimum design variables of the bearing are determined using presented curve fit equations (refer Figs. 9–12 depending upon the type of the bearing and the bearing characteristics to be determined).
4. Find the ratios of maximized force or stiffness generated in multi-ring PMB from the optimization to the maximized force or stiffness generated in a single ring pair bearing configuration from the curve fit equations (refer Figs. 13–16 depending upon the type of the bearing and the bearing characteristics to be determined).

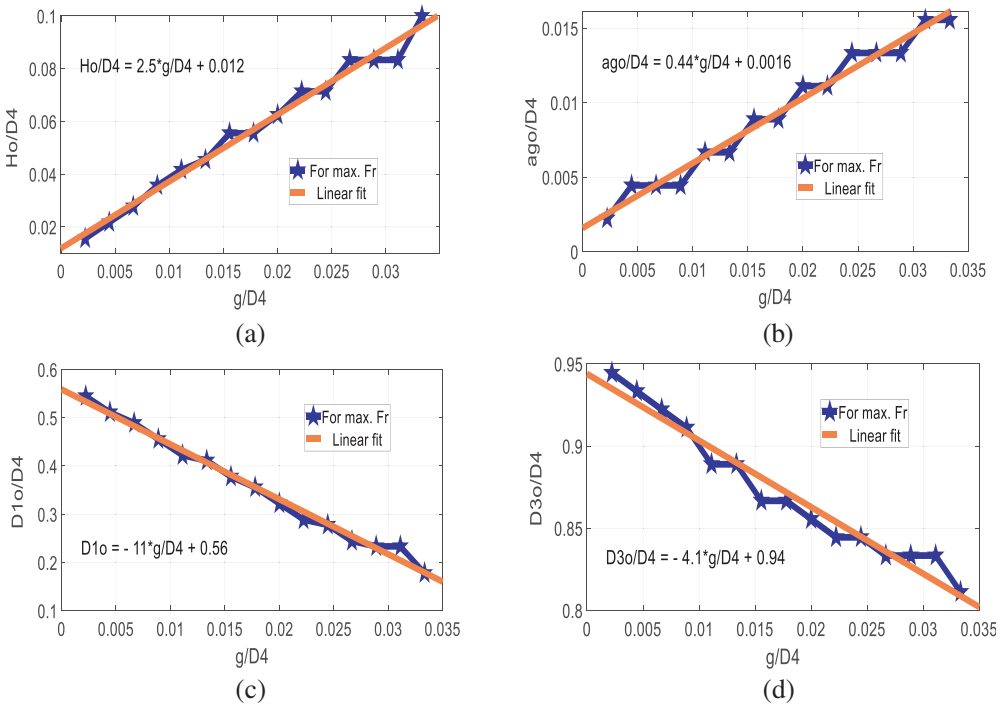

Figure 9. Relationship and curve fit equations for optimum design variables in radial PMB for maximum radial force, (a) Ho/D4 Vs. g/D4, (b) ago/D4 Vs. g/D4, (c) D1o/D4 Vs. g/D4, (d) D3o/D4 Vs. g/D4.

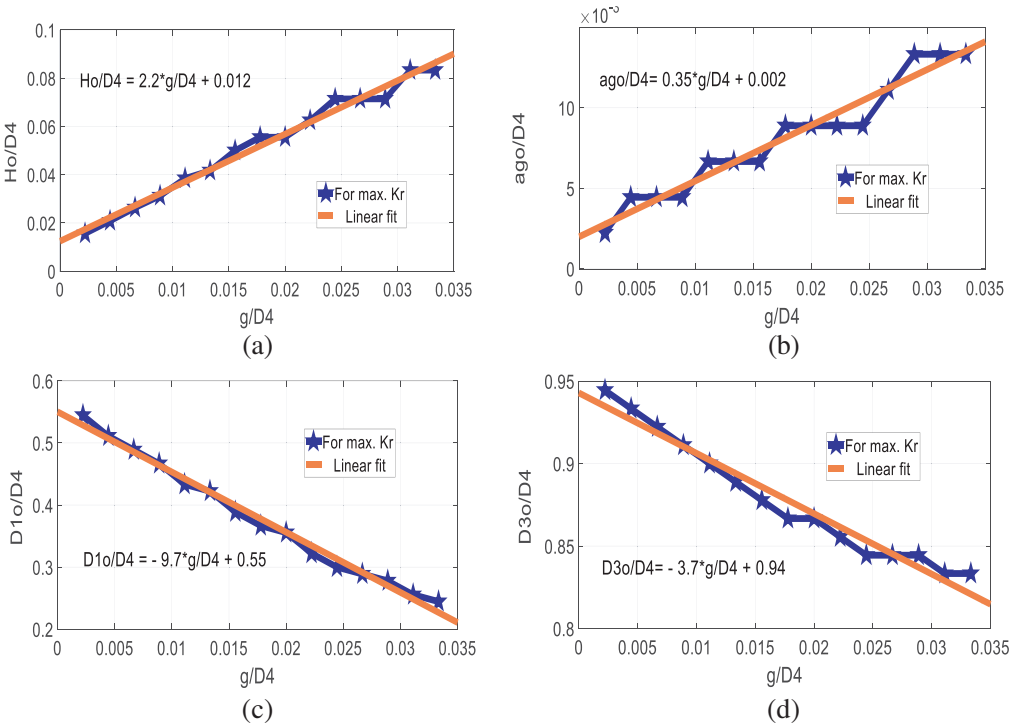

Figure 10. Relationship and curve fit equations for optimum design variables in radial PMB for maximum radial stiffness, (a) Ho/D4 Vs. g/D4, (b) ago/D4 Vs. g/D4, (c) D1o/D4 Vs. g/D4, (d) D3o/D4 Vs. g/D4.

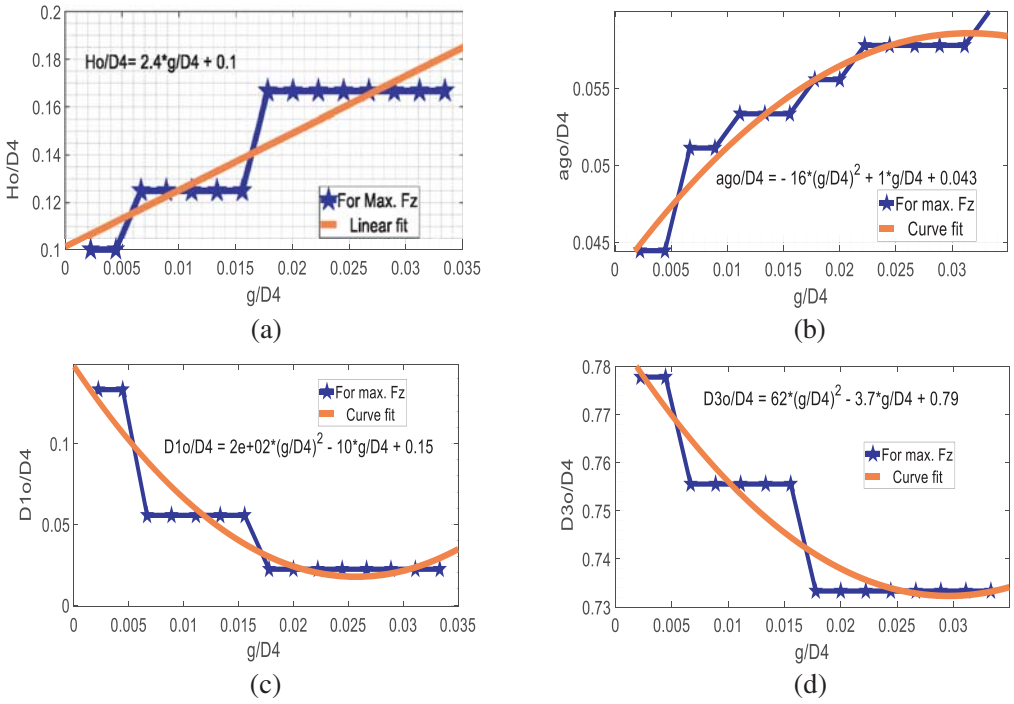

Figure 11. Relationship and curve fit equations for optimum design variables in thrust PMB for maximum axial force, (a) Ho/D4 Vs. g/D4, (b) ago/D4 Vs. g/D4, (c) D1o/D4 Vs. g/D4, (d) D3o/D4 Vs. g/D4.

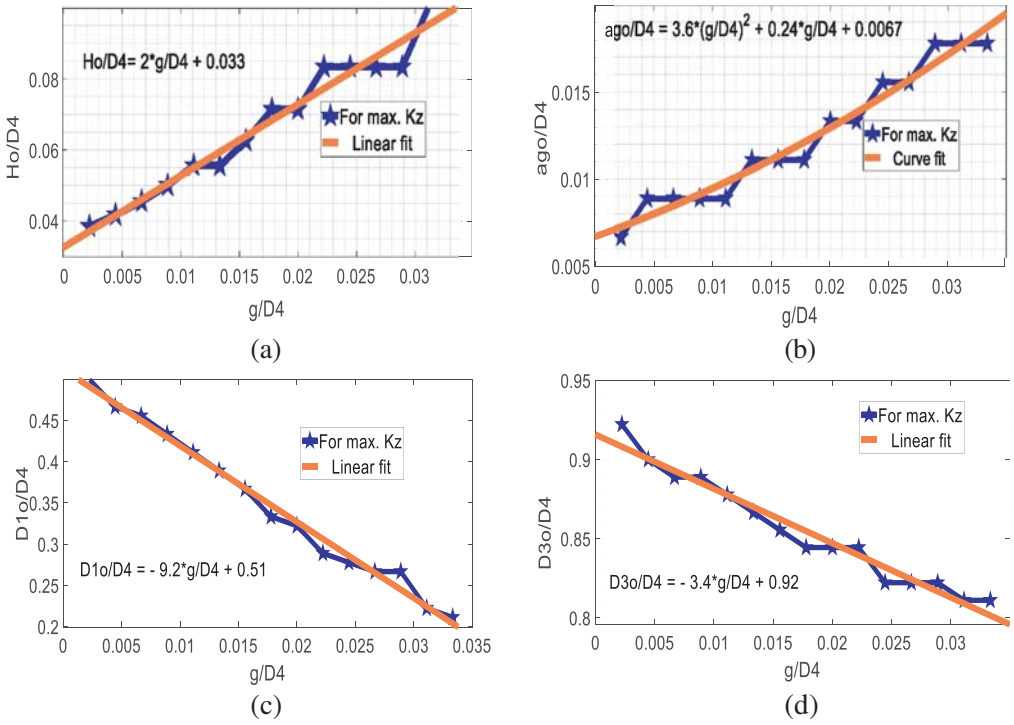

Figure 12. Relationship and curve fit equations for optimum design variables in thrust PMB for maximum axial stiffness, (a) Ho/D4 Vs. g/D4, (b) ago/D4 Vs. g/D4, (c) D1o/D4 Vs. g/D4, (d) D3o/D4 Vs. g/D4.

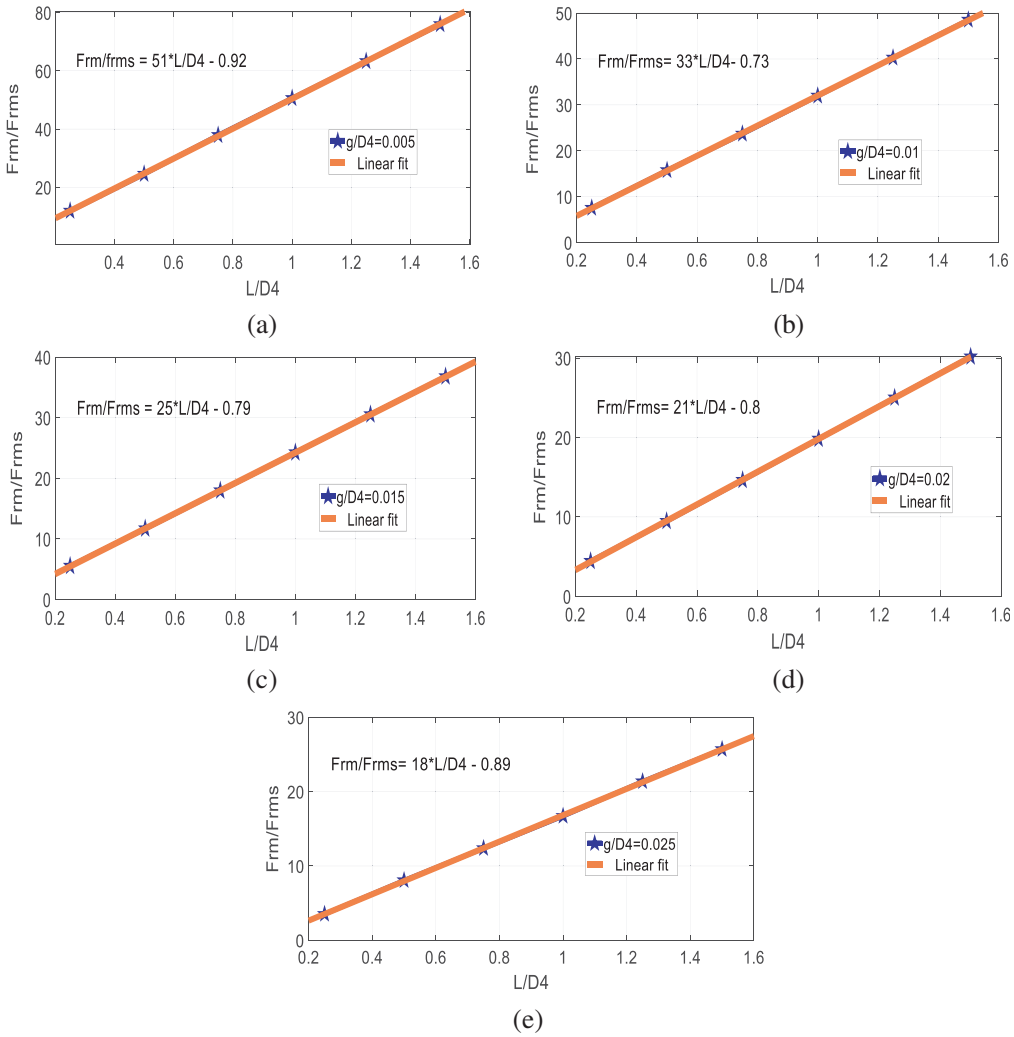

Figure 13. Relationships between Frm/Frms and L/D4 with curve fit equations in radial PMB for (a) g/D4 = 0.005, (b) g/D4 = 0.01, (c) g/D4 = 0.015, (d) g/D4 = 0.02, (e) g/D4 = 0.025.

Table 6. Values of the optimized design variables for maximum radial force (Fr).

g/D4 = 0.02 and L/D4 = 1.0, assume g = 1.75 mm $\Longrightarrow$ D4 = 87.5 mm and L = 87.5 mm		
Optimum parameters	Equations	Optimum values
n_o	Ho/D4 = 2.5(g/D4) + 0.012	Ho = 5.425 and $n_o = 16.12 \approx 16$
ago	ago/D4 = 0.44(g/D4) + 0.0016	ago = 0.91 mm
D1o	D1o = −11(g/D4) + 0.56	D1o = 29.75 mm
D3o	D3o/D4 = −4.1(g/D4) + 0.94	D3o = 75.075 mm
D2o	D2o = D3o − 2g	D2o = 71.575 mm
Frm/Frms	Frm/Frms = 21(L/D4) − 0.8	Frm/Frms = 20.2
Frms	Mathematical model	F_{rms} = 46.42 N
Frmg	Calculation using proposed optimization method	Frmg = 937.71 N
Frmc	Calculation using math. model	Frmc = 916.5 N
% of deviation		2.34

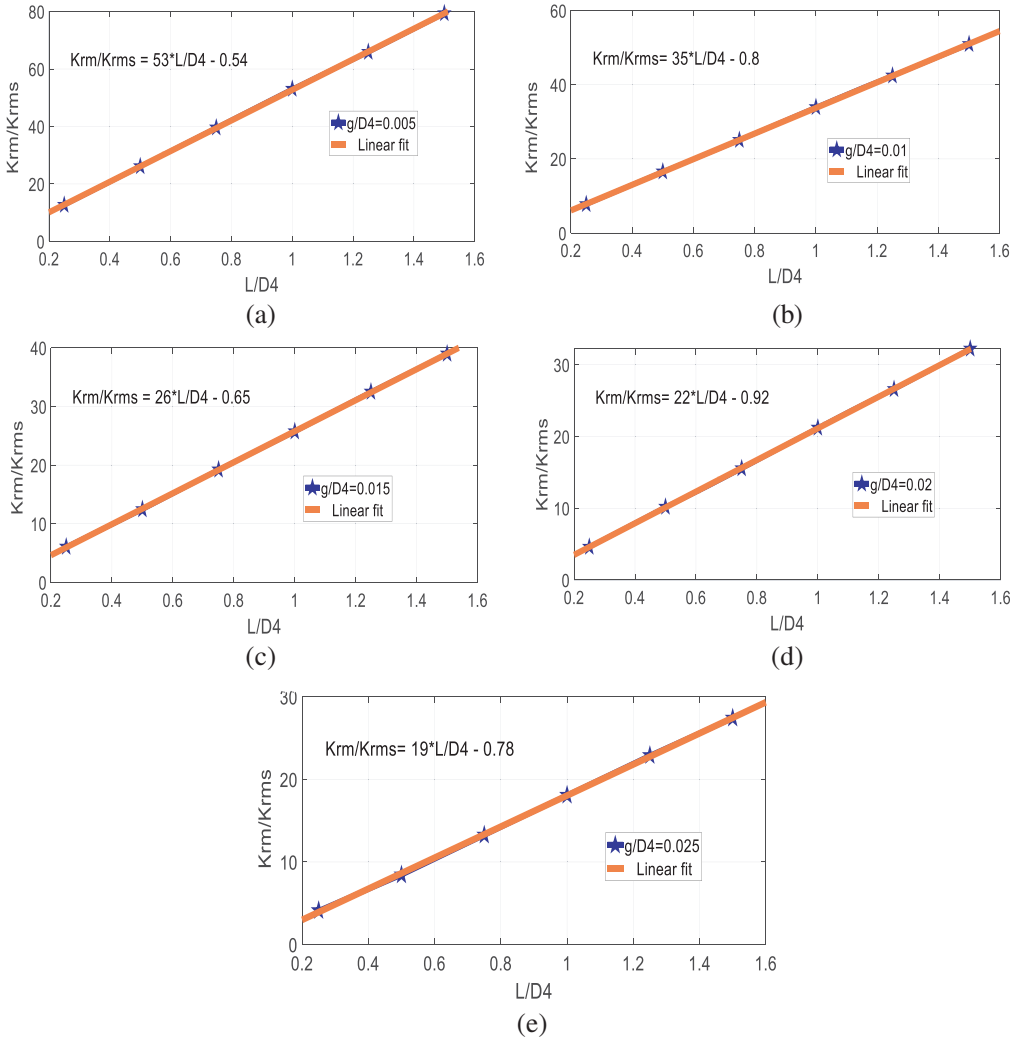

Figure 14. Relationships between Krm/Krms and L/D4 with curve fit equations in radial PMB for (a) g/D4 = 0.005, (b) g/D4 = 0.01, (c) g/D4 = 0.015, (d) g/D4 = 0.02, (e) g/D4 = 0.025.

5. Calculate the maximized force or stiffness generated in a single ring pair bearing configuration from Equations (1) to (4)
6. Finally, the maximum force or stiffness generated in a multi-ring PMB is determined with the value of ratio determined in step 4 and force or stiffness value calculated in step 5.

The radial bearing is to be designed and optimized with g/D4 = 0.02 and L/D4 = 1.0 for maximum radial force or stiffness. By assuming g = 1.75 mm, the optimized values of the design variables and maximized radial force and stiffness are calculated by following the steps listed above in this section. The calculated values of the optimized design variables and the corresponding maximized radial force, and stiffness are given in Tables 6 and 7, respectively. The maximized characteristics of an optimized PMB are also calculated using mathematical equations with the help of optimized design variables. The calculated values are in close agreement with the values calculated using curve fit equations, and deviation is 2.34 and 0.72% respectively for the radial force and stiffness.

The same procedure is also repeated in optimizing the thrust PMB for g/D4 = 0.0125 and L/D4 = 0.75. The value of the air gap assumed in this case is g = 1.25 mm. The results of the optimization procedure and mathematical equations for maximized axial force and stiffness are tabled in Tables 8 and 9, respectively. Deviation in the results using curve fit equations from the mathematical equations for axial force is 6.88%, and for the axial stiffness it is 6%.

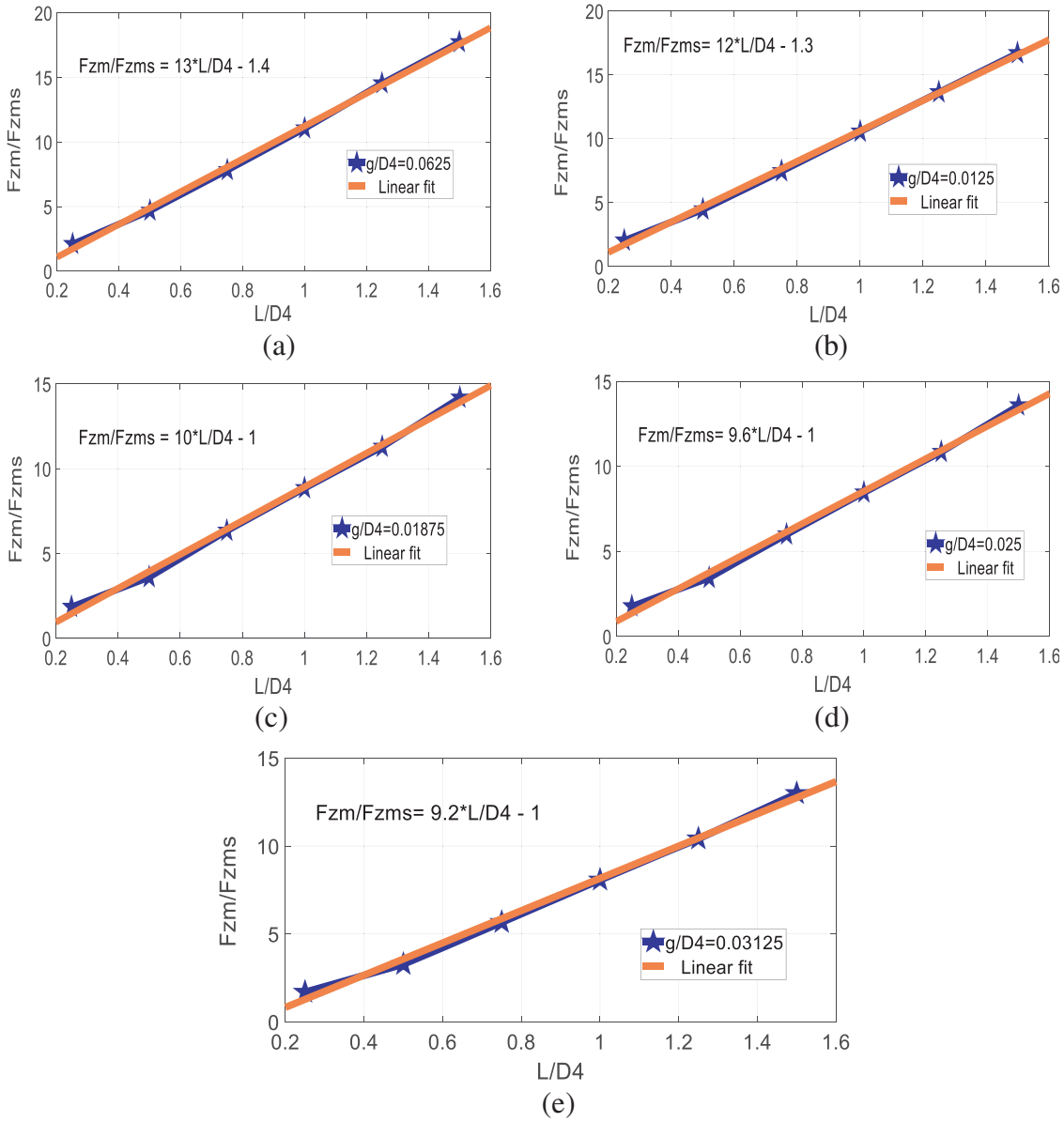

Figure 15. Relationships between Fzm/Fzms and L/D4 with curve fit equations in thrust PMB for (a) g/D4 = 0.005, (b) g/D4 = 0.01, (c) g/D4 = 0.015, (d) g/D4 = 0.02, (e) g/D4 = 0.025.

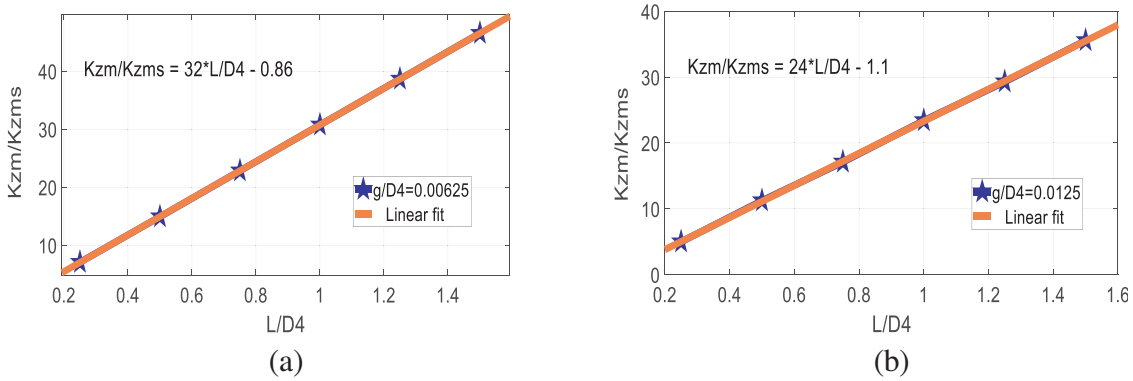

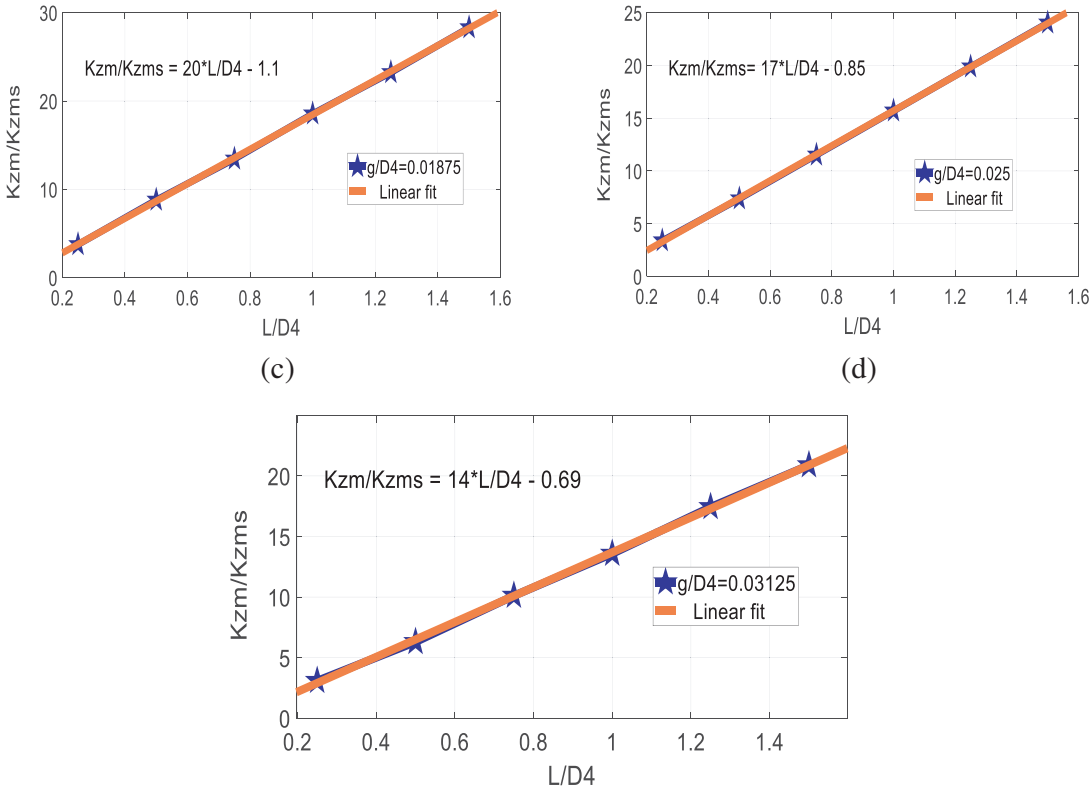

Figure 16. Relationships between Kzm/Kzms and L/D4 with curve fit equations in thrust PMB for (a) g/D4 = 0.005, (b) g/D4 = 0.01, (c) g/D4 = 0.015, (d) g/D4 = 0.02, (e) g/D4 = 0.025.

Table 7. Values of the optimized design variables for maximum radial stiffness (Kr).

g/D4 = 0.02 and L/D4 = 1.0, assume g = 1.75 mm $\Longrightarrow$ D4 = 87.5 mm and L = 87.5 mm		
Optimum parameters	Equations	Optimum values
n_o	Ho/D4 = 2.2(g/D4) + 0.012	Ho = 4.9 mm and $n_o = 17.85 \approx 18$
ago	ago/D4 = 0.35(g/D4) + 0.002	ago = 0.7875 mm
D1o	D1o/D4 = −9.7(g/D4)+ 0.55	D1o = 31.15 mm
D3o	D3o/D4= −3.7(g/D4) + 0.94	D3o = 75.775 mm
D2o	D2o = D3o − 2g	D2o = 72.275 mm
Krm/Krms	Krm/Krms = 22(L/D4) − 0.92	Krm/Krms = 21.08
Krms	Mathematical model	Krms = 5.4535×10^4 N/m
Krmg	Calculation using proposed optimization method	Krmg = 1.14959×10^6 N/m
Krmc	Calculation using math. model	Krmc = 1.1579×10^6 N/m
% of deviation		0.72

Table 8. Values of the optimized design variables for maximum axial force (Fz).

g/D4 = 0.0125 and L/D4 = 0.75, assume g = 1.25 mm $\Longrightarrow$ D4 = 100 mm		
Optimum parameters	Equations	Optimum values
n_o	Ho/D4 = 2.4(g/D_4) + 0.1	Ho = 13 and $n_o = 5.76 \approx 6$
ago	ago/D4 = $-16(g/D_4)^2$ + g/D4 + 0.043	ago = 5.3 mm
D1o	D1o/D4 = 2×10^2 $(g/D4)^2$ − 10(g/D4) + 0.15	D1o = 5.625 mm
D3o	D3o/D4 = $62(g/D4)^2 - 3.7(g/D4) + 0.79$	D3o = 75.343 mm
D2o	D2o = D3o − 2g	D2o = 72.843 mm
Fzm/Fzms	$F_{zm}/F_{zms} = 12(L/D4) - 1.3$	Fzm/Fzms = 7.7
Fzms	Mathematical model	Fzms = 801 N
Fzmg	Calculation using proposed optimization method	Fzmg = 6167.62 N
Fzmc	Calculation using math. model	Fzmc = 5770.07 N
% of deviation		6.88

Table 9. Values of the optimized design variables for maximum axial stiffness (Kz).

g/D4 = 0.0125 and L/D4 = 0.75, assume g = 1.25 mm $\Longrightarrow$ D4 = 100 mm, $\Longrightarrow$ L = 75 mm		
Optimum parameters	Equations	Optimum values
n_o	Ho/D4 = 2(g/D4) + 0.033	Ho = 5.8 mm and $n_o = 12.93 \approx 13$
ago	ago/D4 = $3.6(g/D4)^2$ + 0.24(g/D4) + 0.0067	ago = 1.026 mm
D1o	D1o/D4 = −9.2(g/D4) + 0.51	D1o = 0.395 mm
D3o	D3o/D4 = −3.4(g/D4) + 0.92	D3o = 87.75 mm
D2o	D2o = D3o − 2g	D2o = 85.25 mm
Kzm/Kzms	Kzm/Kzms = 24(L/D4) − 1.1	Kzm/Kzms = 16.9
Kzms	Mathematical model	Kzms = 1.3094×10^5 N/m
Kzmg	Calculation using proposed optimization method	Kzmg = 2.212×10^6 N/m
Kzmc	Calculation using math. model	Kzmc = 2.0829×10^6 N/m
% of deviation		6.0

8. CONCLUSIONS

In this paper, the generalized optimum design methodology for multi-ring radial and thrust PMBs with an axial air gap for maximum force and stiffness in a given volume of the magnet is presented. The following conclusions are based on the present work:

- The single ring pair configuration with the assumed volume of the magnet is analyzed for optimizing multi-ring radial and thrust PMBs using a developed mathematical model. Significant enhancement of force (8.73 and 4.1 times in radial and thrust bearing) and stiffness (9.8 and 7.95 times in radial and thrust bearing) values is seen in both optimized configurations as compared to the monolithic bearing.
- Curve fit equations of the optimum design variables expressed in terms of air gap and equations of maximized force and stiffness expressed in terms of aspect ratio for different values of the air gap

can be used directly in designing and optimizing multi-ring PMB by the designer in the industry.

- The correctness of the proposed optimization procedure is demonstrated by comparing the results of the curve fit equations with the results calculated using a mathematical model. The deviations of 2.34% and 0.72% in force and stiffness in radial bearing and 6.88% and 6% in force and stiffness in thrust bearing with respect to results obtained using mathematical are observed.
- Axial air gaps in the optimized configurations can be used to include conductive material to form ECD to PMB.

ACKNOWLEDGMENT

Authors acknowledge the support provided by Manipal Institute of Technology, Manipal Academy of Higher Education, Manipal and ME Department of National Institute of Technology Karnataka, Surathkal for carrying out the research work.

REFERENCES

1. Baermann, M., "German patent application B," 30042 dated 1954 (German specification No. 1071891).
2. Backers, F. T., "A magnetic journal bearing," *Philips Tech. Rev.*, Vol. 22, 232–238, Jan. 6, 1960.
3. Yonnet, J. P., "Passive magnetic bearings with permanent magnets," *IEEE Trans. Magn.*, Vol. 14, No. 5, 803–805, 1978.
4. Yonnet, J. P., "Permanent magnetic bearings and couplings," *IEEE Trans. Magn.*, Vol. 17, No. 1, 1169–1173, 1981.
5. Ohji, T., et al., "Conveyance test by oscillation and rotation to a permanent magnet repulsive-type conveyor," *IEEE Trans. Magn.*, Vol. 40, No. 4, 3057–3059, 2004.
6. Kriswanto, J., "Radial forces analysis and rotational speed test of radial permanent magnetic bearing for horizontal wind turbine applications," *3rd International Conference on Advanced Materials and Science and Technology (ICAMST 2015), AIP Conference Proceedings, Semarang, Indonesia*, 0200341(1-10), 2015.
7. Sotelo, G. G., R. Andrade, and A. C. Ferreira, "Magnetic bearing sets for a Flywheel system," *IEEE Trans. on Applied Super Conductivity*, Vol. 17, No. 2, 2150–2153, 2007.
8. Fang, J., Y. Le, J. Sun, and K. Wang, "Analysis and design of passive magnetic bearing and damping system for high-speed compressor," *IEEE Trans. Magn.*, Vol. 48, No. 9, 2528–2537, 2012.
9. Le, Y., J. Fang, and J. Sun, "Design of a Halbach array permanent magnet damping system for high speed compressor with large thrust load," *IEEE Trans. Magn.*, Vol. 51, No. 1, 1–9, 2015.
10. Bekinal, S. I., S. Jana, and S. S. Kulkarni, "A hybrid (permanent magnet and foil) bearing set for complete passive levitation of high-speed rotors," *Proc. IMechE, Part C: J. Mechanical Engineering Science*, Vol. 231, 3679–3689, 2017.
11. Bekinal, S. I. and M. Doddamani, "Friction-free permanent magnet bearings for rotating shafts: A comprehensive review," *Progress In Electromagnetics Research C*, Vol. 104, 171–186, 2020.
12. Paden, B., N. Groom, and J. Antaki, "Design formulas for permanent-magnet bearings," *ASME Trans.*, Vol. 125, 734–739, 2003.
13. Tan, Q., W. Li and B. Liu, "Investigations on a permanent magnetic hydrodynamic journal bearing," *Tribology International*, Vol. 35, 443–448, 2002.
14. Samanta, P. and H. Hirani, "Magnetic bearing configurations: Theoretical and experimental studies," *IEEE Trans. Magn.*, Vol. 44, No. 2, 292–300, 2008.
15. Lijesh, K. P. and H. Hirani, "Development of analytical equations for design and optimization of axially polarised radial passive magnetic bearing," *ASME Journal of Tribology*, Vol. 137, 011103(1-9), 2015.
16. Ravaud, R., G. Lemarquand, and V. Lemarquand, "Halbach structures for permanent magnets bearings," *Progress In Electromagnetics Research M*, Vol. 14, 263–277, 2010.

17. Bekinal, S. I., A. R. Tumkur Ramakrishna, S. Jana, S. S. Kulkarni, A. Sawant, N. Patil, and S. Dhond, "Permanent magnet thrust bearing: Theoretical and experimental results," *Progress In Electromagnetics Research B*, Vol. 56, 269–287, 2013.
18. Tian, L.-L., X.-P. Ai, and Y.-Q. Tian, "Analytical model of magnetic force for axial stack permanent-magnet bearings," *IEEE Trans. Magn.*, Vol. 48, No. 10, 2592–2599, 2012.
19. Bekinal, S. I. and S. Jana, "Generalized three-dimensional mathematical models for force and stiffness in axially, radially, and perpendicularly magnetized passive magnetic bearings with 'n' number of ring pairs," *ASME Journal of Tribology*, Vol. 138, No. 3, 031105(1-9). 2016.
20. Moser, R., J. Sandtner, and H. Bleuler, "Optimization of repulsive passive magnetic bearings," *IEEE Trans. Magn.*, Vol. 42, No. 8, 2038–2042, 2006.
21. Lijesh, K. P., M. R. Doddamani, and S. I. Bekinal, "A pragmatic optimization of axial stack-radial passive magnetic bearings," *ASME Journal of Tribology*, Vol. 140, 021901(1–9), 2018.
22. Lijesh, K. P., M. R. Doddamani, S. I. Bekinal, and S. M. Muzakkir, "Multi-objective optimization of stacked radial passive magnetic bearing," *Proc. IMechE Part J: J. Engineering Tribology*, Vol. 232, 1140–1159, 2018.
23. Van Beneden, M., V. Kluyskens, and B. Dehez, "Optimal sizing and comparison of permanent magnet thrust bearings," *IEEE Trans. Magn.*, Vol. 53, No. 2, 1–10, 2017.
24. Bekinal, S. I., M. R. Doddamani, and S. Jana, "Optimization of axially magnetised stack structured permanent magnet thrust bearing using three dimensional mathematical model," *ASME Journal of Tribology*, Vol. 139, No. 3, 031101(1-9), 2017.
25. Bekinal, S. I., M. R. Doddamani, B. V. Mohan, and S. Jana, "Generalized optimization procedure for rotational magnetized direction permanent magnet thrust bearing configuration" *Proc. IMechE, Part C: J. Mechanical Engineering Science*, Vol. 233, 2563–2573, 2019.
26. Sodano, H. A. and D. J. Inman, "Modeling of a new active eddy current vibration control system," *ASME Journal of Dynamic Systems, Measurement and Control*, Vol. 130, 021009-1-11. 2008.
27. Detoni, J. G., Q. Cui, N. Amati, and A. Tonoli, "Modelling and evaluation of damping coefficient of eddy current dampers in rotordynamic applications," *Journal of Sound and Vibration*, Vol. 373, 52–65, 2016.
28. Passenbrunner, J., G. Jungmayr, and W. Amrhein, "Design and analysis of a 1d actively stabilized system with viscoelastic damping support," *Actuators*, Vol. 8, No. 33, 2–18, 2019.
29. Yoo, S. Y., W. Kim, S. Kim, W. Lee, Y. Bae, and M. Noh, "Optimal design of non-contact thrust bearing using permanent magnet rings," *Int. Journal of Precision Engg. and Manufacturing*, Vol. 12, No. 6, 1009–1014, 2011.
30. Safaeian, R. and H. Heydari, "Comprehensive comparison of different structures of passive permanent magnet bearings," *IET Electric Power Appl.*, Vol. 12, 179–187, 2017.
31. Bekinal, S. I. and M. Doddamani, "Improvement in the design calculations of multi ring permanent magnet thrust bearing," *Progress In Electromagnetics Research M*, Vol. 94, 83–93, 2020.